# 2 Group V endohedral fullerenes

Nitrogen in the $C_{60}$ Buckminster fullerene was first discovered in 1995 by the group of A. Weidinger at the Hahn–Meitner institute in Berlin [1]. A short time later also phosphorous in $C_{60}$ could be produced [2]. It has been calculated for nitrogen [3] as for phosphorous [4], that the wavefunction of the atom does not mix with the wavefunction of the fullerene molecule. Thus, none of the usually highly reactive atoms binds to the $C_{60}$ cage. This is supported by ESR and (only for nitrogen) ENDOR measurements, which show only atomic spectra with isotropic hyperfine interactions as expected for the quartet ground state of the electron spin[5] [1-7].

Both endohedral fullerenes are stable at room temperature. N@$C_{60}$ can be heated up to 450 K without losing the endohedral atom while P@$C_{60}$ gets unstable at 400 K [8]. Up to now, three different types of chemical reactions have been shown to leave the endohedral atom unchanged: mechano-chemical synthesis of the N@$C_{60}$-$C_{60}$ dimer [9] and the "Bingel" reaction e.g. the N@$C_{61}(COOC_2H_5)_2$ mono-adduct [10]. With the production of N@PCBM, we could show recently that even reactions with much higher enthalpy may leave the endohedral atom unchanged (see appendix A). PCBM is a fullerene modification [11] used as acceptor in organic solar cells [12]. Its production involves annealing at high temperature (80°C) for ~ 8 h as well as strong acid treatment.

The linewidths of N/P@$C_{60}$ highly diluted in a $C_{60}$ matrix are less than 1 µT, indicating very long relaxation times. One can say that $C_{60}$ serves as a container for one electron spin that is very well shielded from the surrounding. This feature of the group V endohedral fullerenes turns them into interesting candidates for qubits in a quantum computing scheme.

## 2.1 Production

Endohedral fullerenes can be produced either during the growth process of the fullerenes or afterwards. For metallofullerenes as La@$C_{82}$ [13], the graphite rods in the Krätschmer–Huffman method are doped with metal oxides or metal carbides. Nobel gas endohedrals are formed in a high pressure gas atmosphere during annealing due to the window mechanism [14].

The methods described above can be used only with non-reactive atoms. Alkali metals [15] and the highly reactive group V atoms have to be produced by ion implantation.

[5] the three p – shell electrons couple to a spin S = 3/2 with quantum number $\ell = 0$.

### 2.1.1 Ion implantation

The endohedral fullerenes are produced by ion implantation in high vacuum as drafted in Fig. 2.1. $C_{60}$ fullerenes are evaporated from a boron–nitrite effusion cell at ~ 770 K. The deposition rate used is usually ~ 20 Å/s causing a pressure of $10^{-4}$ mbar.

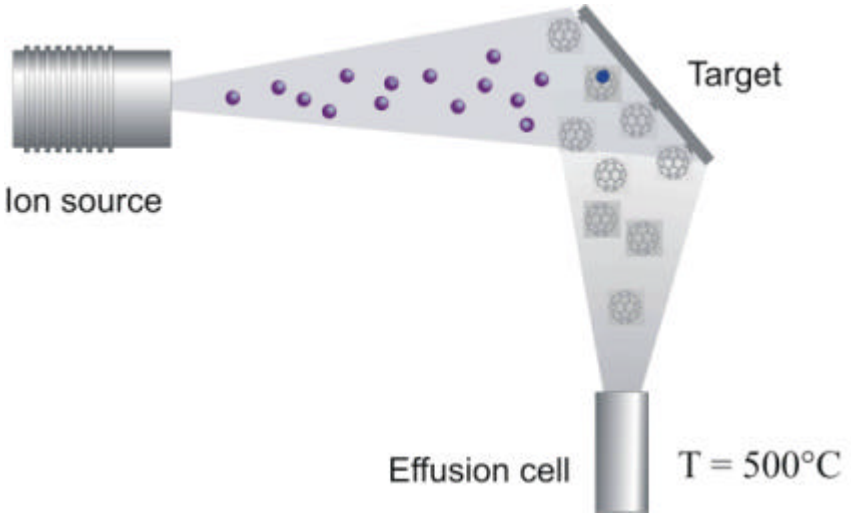


*Fig. 2.1: Scheme of the ion implantation of phosphorous or nitrogen in $C_{60}$. Fullerenes are evaporated at ~ 770 K. At the same time, charged ions of an $N_2$ or $PH_3$ plasma are accelerated towards a target cooled to ~ 230 K. The flux is adjusted such that a fresh monolayer of $C_{60}$ is irradiated with a sufficient number of ions.*

For the generation of the ions a high frequency plasma source HFQ 1303-3 of Plasma Consult is used with $N_2$ or $PH_3$. The low energy ions (~ 40 eV [5]) hit the fullerene molecules at a copper target. As the penetration depth of the ions in the $C_{60}$ film is only a few mono–layers, the ion current has to be adjusted to the evaporation rate of the $C_{60}$. In this way every fullerene mono–layer is irradiated with ions before the next layer is deposited.

The temperature of the target turned out to be the most important parameter for the implantation efficiency. In order to dissipate the vibration energy of the $C_{60}$ molecules hit by an implantation ion, the copper target has been cooled to ~ 230 K.

### 2.1.2 Characterisation and enrichment

After the implantation the powder is dissolved in toluene. To check the quality of the material, the concentration of fullerene molecules and the number of spins have to be determined. First, the concentration of $C_{60}$ fullerenes is measured by the UV absorption in an HPLC (high pressure liquid chromatography) experiment. Afterwards, 50 µl of the solution are measured in an cw ESR experiment. The integrated intensity of the resonance line is proportional to the number of spins in the sample. A film of sputtered silicon with $1.4 \cdot 10^{14}$ spins has been used for calibration. The best ratio of filled to empty fullerenes that could be reached was $3 \cdot 10^{-4}$.

Most experiments work well with this quality. However, a quantum computer requires purified N/P@$C_{60}$. For N@$C_{60}$ it has been shown recently, that purification with HPLC is possible [16]. With a high pressure valve, N@$C_{60}$ dissolved in toluene is injected in the solvent circuit. This mixture flows with a rate of 12.5 ml/min through a column (Waters Buckyprep, 250mm x 50mm) that builds up a pressure of 80 bar. Due to the difference in polarisability, the nitrogen filled $C_{60}$ molecules leave the column with an additional retention time of 30 s compared to the empty fullerenes.

As the main subject of this work is P@$C_{60}$, first the retention time of this material had to be determined. This has been done in an HPLC experiment similar to that described above. As the retention time of the phosphorous filled fullerenes was not known, 10 fractions where collected, each 10 seconds long. The HPLC chromatogram is shown in Fig. 2.2.

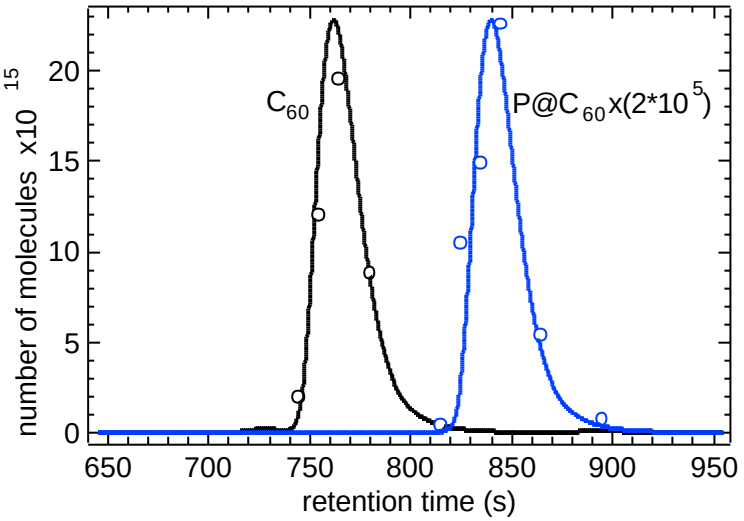


*Fig. 2.2: The Retention time of P@$C_{60}$ compared to $C_{60}$ can be measured by taking fractions every 10 seconds. The number of $C_{60}$ molecules is measured directly by the absorption signal, while the number of endohedral fullerenes is determined via the number of spins by ESR.*

The number of $C_{60}$ molecules has been determined via the intensity of the UV absorption at a wavelength of $\lambda$ = 280 nm. The P@$C_{60}$ signal could be reconstructed after the number of spins in each fraction had been determined. As can be seen in Fig. 2.2, the retention time of P@$C_{60}$ is about 80 seconds longer compared to $C_{60}$. This is much more than the 30 seconds for N@$C_{60}$, indicating that P@$C_{60}$ has a higher polarisability. This leads to an enrichment factor of more than 30 per HPLC cycle making the enrichment much faster for P@$C_{60}$ than for N@$C_{60}$.

## 2.2 Phosphorous in $C_{60}$

Since phosphorous is in the same column of the periodic table as nitrogen and the configuration of the outer electron shells is the same, P@$C_{60}$ is expected to have similar properties as N@$C_{60}$. However, the larger van der Waals radius of phosphorous of 1.7

Å (N: 1.55 Å), the lower ionisation potential of 10.5 eV (N: 14.5 eV), and the positive electron affinity of 0.74 eV (N: -0.32 eV) tend to increase the interaction of the encapsulated atom with the fullerene shell. Therefore, a lot of properties of the group V endohedral fullerenes show up more distinctly in P@$C_{60}$, e.g. the relaxation properties discussed in chapter 3, and the polarisability as shown before.

In the left part of Fig. 2.3 the ESR spectrum of a P@$C_{60}$ powder sample is shown. The two hyperfine lines give no sign of any anisotropic broadening. The value of the electron g factor $g_e$ is scalar and nearly that of the free electron. The hyperfine interaction is completely isotropic even in solid state and therefore the hyperfine constant a is scalar, too. The Hamiltonian describing the spin system can be written as

$$H = g_e m_B S B_0 - g_N m_N I B_0 + aIS \qquad (2.1)$$

with the nuclear g value $g_N$ and the magnetic moment $\mu_N$ of the nuclear spin I. Since the nuclear Zeeman energy is very small compared to the energy of the electron Zeeman effect, it can be disregarded in the analysis of ESR spectra.

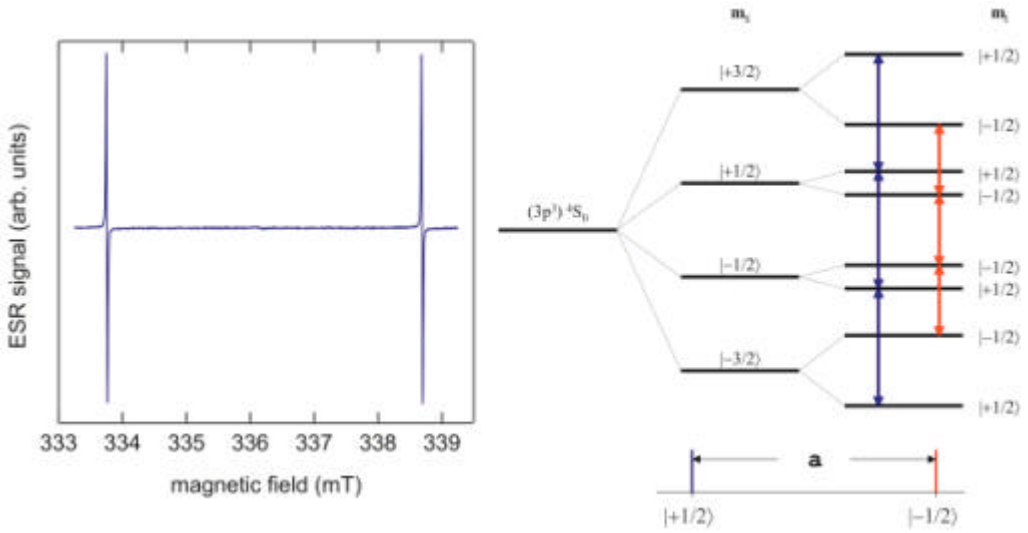


*Fig. 2.3: The left part shows the ESR spectrum of a P@$C_{60}$ powder sample. The cw measurement was carried out at room temperature with micro wave power of 63 µW and modulation amplitude 20 µT. Two hyperfine lines arise due to the nuclear spin $m_I$ = 1/2 of $^{31}$P as demonstrated in the energy level diagram in the right part. The hyperfine splitting is $a/g_e \mu_B$ = 4.9 mT.*

With the Paschen–Back approximation ($g_e \mu_B S B_0$ >> aIS), equation (2.1) results in energy levels shown in the right part of Fig. 2.3. Only two hyperfine lines without any fine structure are visible. With $a/g_e \mu_B$ = 4.9 mT the hyperfine coupling of P@$C_{60}$ is about 120% larger than for the free phosphorous atom [18] (for nitrogen the difference is just 30%). This indicates that the electron wavefunction of the endohedral atom is squeezed by the fullerene molecule, enhancing the interaction between the electron and the nuclear spin.

As can be seen in Fig. 2.4, the hyperfine lines of P@$C_{60}$ in solution show a three–fold splitting. This is due to second order hyperfine interaction which leads to a splitting for

hyperfine lines with $m_I \neq 0$ of $a^2/2g_e\mu_B B_0$ = 36 µT [17]. Although this splitting is expected in powder samples, too, only non–split hyperfine lines can be measured.

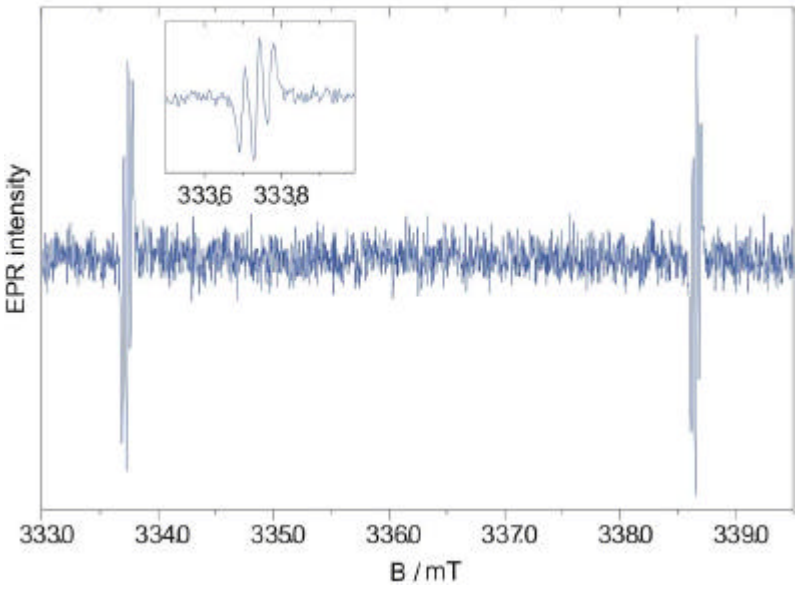


*Fig. 2.4: ESR spectrum of P@$C_{60}$ in solution done in [17]. The splitting of the hyperfine lines is due to second order effects.*

In order to solve this contradiction, the solution and powder spectra of the same sample (ratio of filled to empty fullerenes 8.6 ·$10^{-4}$) have been measured. The results are shown in Fig. 2.5. Both spectra were measured with a cw–ESR spectrometer (Miniscope 100, Magnettech) at 30µW mircowave power and with 0.1 mT modulation amplitude.

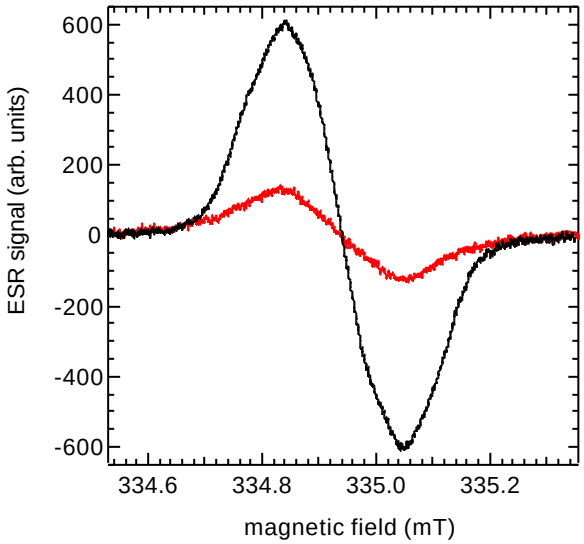


*Fig. 2.5: Solution (black line) and powder (red line) spectrum of the $m_I$ =1/2 hyperfine line of the same sample. The measurements were done at room temperature with 30 µW microwave power and 0.1 mT modulation amplitude. Because of the large modulation amplitude, the different ESR transitions are not resolved anymore.*

The different ESR transitions are not resolved anymore due to this large modulation amplitude. Nevertheless, the integrated intensity of both lines should be the same. But the integrated intensity of the sample in solution is larger than that of the powder sample by a factor of three. Thus, at room temperature in the spectrum of P@$C_{60}$, only the (1/2, -1/2) transitions are visible. As examined and discussed in chapter 4.4 (pp. 51 et sq.), a zero–field splitting SDS with a distribution of D values in combination with relaxation is the reason for the "vanishing" of the (±3/2, ±1/2) transitions.

In N@$C_{60}$ fluctuations of the hyperfine coupling are known to be the major source for relaxation [19]. Therefore and in view of the relaxation measurements in chapter 3, we will now have a closer look at the hyperfine coupling of P@$C_{60}$. This is done with FT–ESR measurements as follows:

A short (12 ns) microwave pulse ($B_1$ ~ 1 mT) is applied perpendicular to $B_0$. The magnetisation is rotated to the x,y–plane and decays exponentially due to dephasing. An example for this transient signal, called Free Induction Decay (FID), is shown in Fig. 2.6 (a).

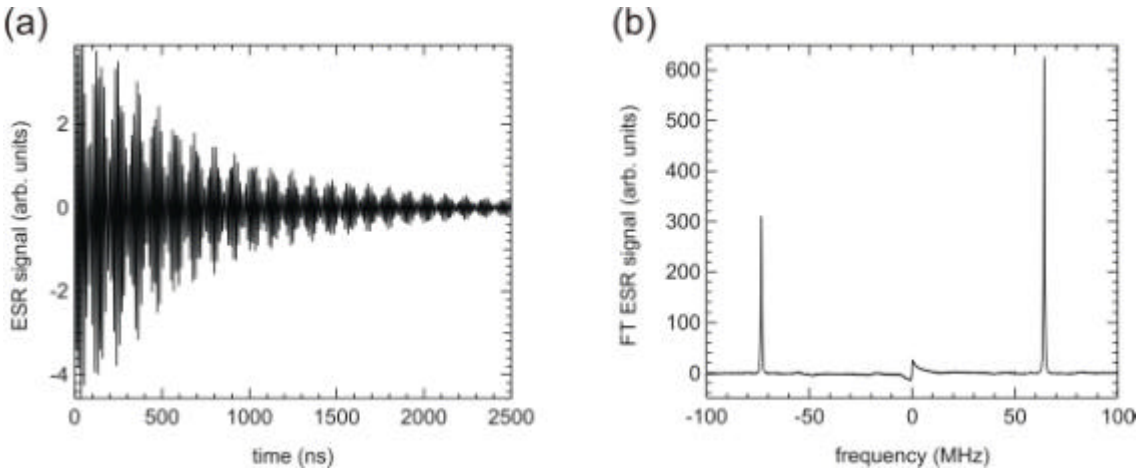


*Fig. 2.6: (a) Fraction of the 8 µs FID of P@$C_{60}$ at 100 K measured after a 12 ns pulse. The fast oscillation is due to the applied magnetic field $B_0$ chosen off-resonance for both hyperfine lines. As the resonance lines lie asymmetrically around $B_0$ , a beat superimposes the oscillation.*

*(b) The Fourier transformation of the FID after phase correction reveals the spectrum of P@$C_{60}$ with two hyperfine lines. The frequency width of the sinc-shaped exciting pulse is 166 MHz. As the excitation is not exactly in the middle between the resonance lines, the amplitude of the hyperfine lines separated by 137.5 MHz appears to be different.*

Oscillations are due to a mismatch between the angle velocity of the rotating frame of the detection and the Larmor–frequency of the resonance. The FID contains the whole information about the spectrum that is gained after Fourier transformation of the ESR signal. This is shown in Fig. 2.6 (b). The small kink at zero frequency is an artefact of the transform. As the transient signal has to be cut off at some point, small frequencies corresponding to (infinitely) long times cannot be obtained from the FID. A short but

nice introduction into pulse and Fourier–Transform magnetic resonance can be found in [20].

The temperature dependence of the isotropic hyperfine splitting $a/2\pi h$ of $P@C_{60}$ is shown in Fig. 2.7. At temperatures T < 35 K the hyperfine coupling is constant. With rising temperature it increases continuously. This can be explained assuming that at low temperatures the atom is in its vibrational ground state, and that at higher temperatures vibrational states are excited.

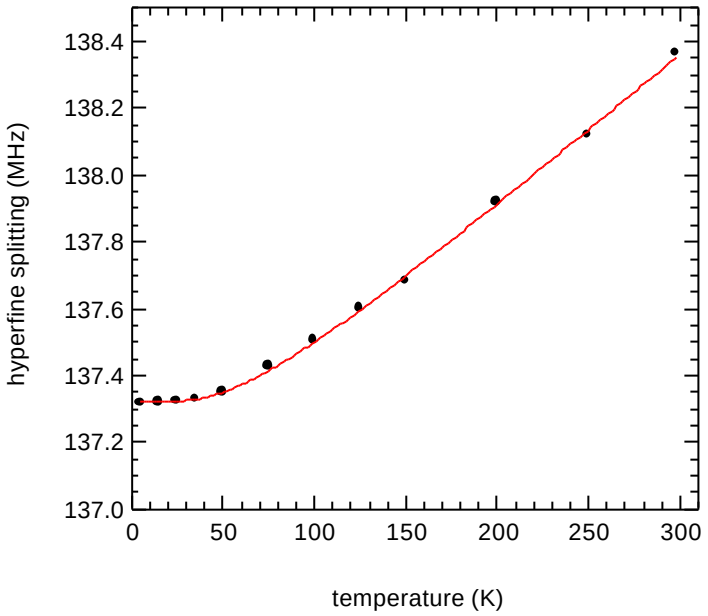


*Fig. 2.7: Temperature dependence of the hyperfine coupling constant (black markers) of $P@C_{60}$ and fit with the theoretical characteristics of the mean square displacement of phosphorous in its $C_{60}$ cage.*

The excitation of vibrational states causes a larger wavefunction overlap between the $C_{60}$ shell and the endohedral atom, and thus an increase of the hyperfine coupling as discussed for $N@C_{60}$ in [19]. In case of the three dimensional harmonic oscillator with the quantum number $n = n_x + n_y + n_z$, the hyperfine coupling constant $A$ can be developed as

$$A(n) = \tilde{A}_0 + \Delta A\left(n + \frac{3}{2}\right). \tag{2.2}$$

The average hyperfine coupling constant is

$$A(T) = \sum_{n=0}^{\infty} P_n(T) \cdot A(n), \tag{2.3}$$

where $P_n(T)$ the temperature dependent population probability of state $n$. Assuming a Boltzmann distribution for the population of the excited vibrational states

$$P_n(T) = \frac{(n+1)(n+2)\cdot \exp\left(-\frac{nh\nu_0}{kT}\right)}{\sum_{n=0}^{\infty}(n+1)(n+2)\cdot \exp\left(-\frac{nh\nu_0}{kT}\right)} \qquad (2.4)$$

for the three dimensional oscillator, and using (2.3) with (2.2) and (2.4), we obtain

$$A(T) = A_0 + \Delta A \frac{1}{\exp\left(\frac{h\nu_0}{kT}\right)-1} \qquad (2.5)$$

with $A_0 = \tilde{A}_0 + \frac{3}{2}\Delta A$.

The fit of the data in Fig. 2.7 with (2.5) yields an oscillator energy of $h\nu_0$ = 15(1) meV and the hyperfine coupling constant corresponding to this state $A_0/2\pi h = a_0/2\pi h$ = 137.32 (0.05) MHz.

In ref. [4], the potential of phosphorous encapsulated in $C_{60}$ has been computed with Hartree – Fock calculations. The oscillator energy is in close agreement with the experimental results, and nearly the same as in N@$C_{60}$ ($h\nu_0$ = 13(1) meV, [19]).

The hyperfine coupling of phosphorous trapped in $C_{60}$ is about 120% stronger than for a free phosphorous atom [21]. As expected from the larger van der Waals radius, this is much more than in the case of N@$C_{60}$, where the hyperfine coupling is increased only by 20%. However, the temperature dependence is similar and due to vibrations of the atom in the $C_{60}$ molecule.

## 2.3 N@$C_{60}$ and P@$C_{60}$ as Qubits

Since the hyperfine coupling of nitrogen and phosphorous in $C_{60}$ is so different, their resonance lines in ESR are very well separated and can be excited selectively. In quantum computing terms one would say that they can be addressed separately and fulfil DiVincenzo's first criterion (see chapter 1).

However, to decide whether the endohedral spins could serve as qubits in a quantum computing scheme, the third criterion – long coherence time $T_{coh}$ compared to the gate operation time – has to be matched, as well. This means that the coupling J between the spins has to be strong enough, so $h/2J << T_{coh}$.

### 2.3.1 Coupling

Until today no evidence of exchange coupling has been found even in pure N@$C_{60}$. The only interaction between the spins is magnetic dipolar coupling. Therefore, the coupling between two electron spins S (for $g_e\mu_B B_0 >> J$) can be described as

$$H_{coup} = J(r, J) S_{1z} S_{2z}, \qquad (2.6)$$

where

$$\frac{J(r,J)}{h} = \left(\frac{m_0}{4p}\right)\frac{g^2 h}{r^3}\frac{1}{2}\left(1-3\cos^2 J\right) \qquad (2.7)$$

giving J/h ~ 52 MHz for $\delta = 0°$ and $r_j = 1$ nm (see Fig. 2.8) corresponding to the lattice constant in a fullerene crystal. Here, $\gamma$ is the gyromagnetic ratio of the electron and $\mu_0$ the vacuum permeability.

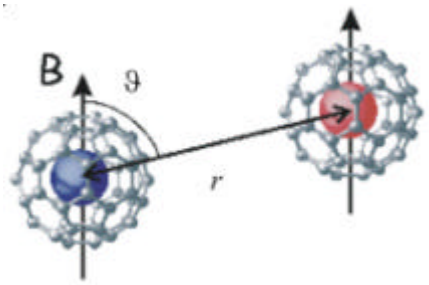


*Fig. 2.8: The dipolar coupling between two endohedral spins depends on the distance $r_j$ and the angle d of their connecting axis with respect to the magnetic field.*

As demonstrated in [19], the linewidth of a powder spectrum depends strongly on the spin concentration and hence on the dipolar interaction between the spins. It is shown in Fig. 2.9 that already for a powder sample of ~ 8% spin concentration the hyperfine lines become indistinct.

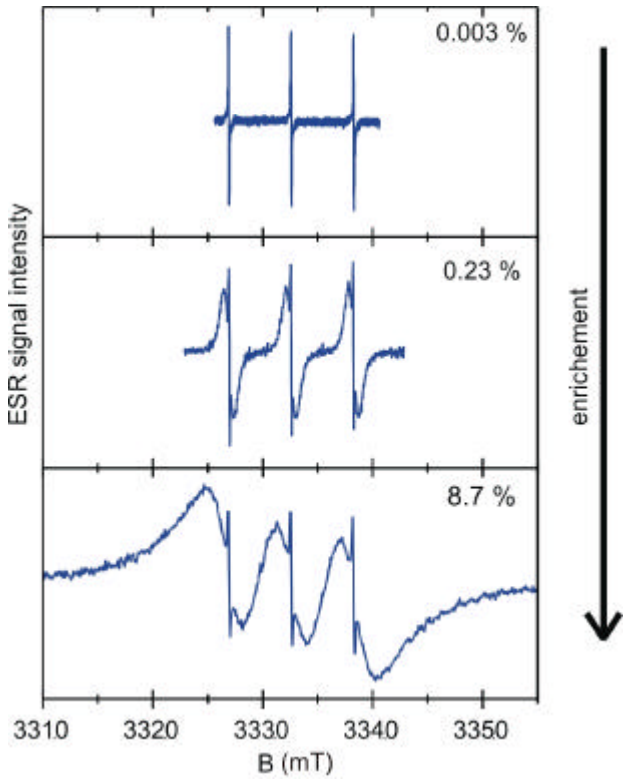


*Fig. 2.9: Powder spectra of N@$C_{60}$ in $C_{60}$ after different steps of enrichment. The line broadening is due to dipolar coupling between the endohedral spins. The results are taken from [19].*

For quantum computing this means that one has to work either with a gated QC as described in the previous chapter. In this case one works with single spins which do not cause line broadening. On the other hand, ensemble computing can be done if all quantum registers (see chapter 1) are oriented in the same direction and thus all spins have the same strength of interaction. This would lead only to a shift of the resonance lines

### 2.3.2 Decoherence

The ESR linewidth measured in cw experiments is not only an indication for the strength of the dipolar interaction but also for the spin relaxation times. In the case of slow passage through the resonance (the system is in equilibrium at every time), the linewidth Γ can be derived from the Bloch–equations [22]

$$\Gamma = \frac{2}{T_2}\sqrt{1+g^{2}B_1^2T_1T_2}\ , \tag{2.8}$$

with γ the gyromagnetic ratio of an electron, $B_1$ the amplitude of the applied microwave, $T_1$ the spin–lattice and $T_2$ the spin–spin relaxation time (definition see chapter 3). For cw measurements usually $g_e^2B_1^2T_1T_2 << 1$ applies and equation (2.8) reduces to

$$\Gamma \approx \frac{2}{T_2}. \tag{2.9}$$

As $T_2$ corresponds to the phase coherence in an ensemble, broad lines usually indicate strong decoherence. For samples of $N@C_{60}$ with a quality of $1\cdot10^{-4}$ in cw experiments a linewidth of ~ 4.8 µT has been measured. With equation (2.9) this is expected to result in a relaxation time $T_2$ = 14 .8 µs. The measured value of the spin–spin relaxation time is $T_2$ = 14 µs [19], which is in very good agreement with the prediction.

For powder samples with a higher spin concentration, much shorter relaxation times are expected as the dipolar coupling between the electron spins is the main spin–spin relaxation mechanism for $N@C_{60}$ and $P@C_{60}$, respectively. But this will not apply for a quantum computer.

As described before, the dipolar coupling will be controlled in a quantum computing scheme in order to serve as qubit interaction. Since adjacent spins will have different resonance frequencies (due to different type of endohedral atom or a field–gradient) and are thus "unlike" spins, spin diffusion, also called "flip–flop" term, is suppressed. As long as no other mechanism causes relaxation, the phase coherence in a quantum computer built from endohedral fullerenes can equal the spin lattice relaxation time $T_1$ with seconds.

The maximum coupling is $J_{max}/h$ ~ 52 MHz, which leads to a gate operation time of $T_{gate}$= h/2J = 10 ns. The factor that shows how many operations can be done before dephasing is then $T_{coh}/T_{gate} = 1\cdot10^{8}$. Even if the maximum $T_2$ would be only 14 µs, it still allows 1400 operations, which is more than sufficient for a proof of concept.

Experiments and a more detailed discussion about the relaxation times and mechanisms follow in the next chapter.

## 2.4 Conclusions

The properties of $N@C_{60}$ have been reviewed with respect to the application as qubit in the quantum computer scheme presented in chapter 1. Relaxation times and coupling strength allow about 1400 operations. This is more than sufficient for a proof of concept.

The hyperfine coupling of $P@C_{60}$ is much larger than for $N@C_{60}$. However, the temperature dependence of the two endohedral fullerenes is similar. Both group V endohedral fullerenes show a harmonic potential for the endohedral atom, though the potential seems to be slightly steeper for phosphorous. Therefore, the phosphorous atom is expected to reside at the centre of the $C_{60}$ molecule as predicted by [23, 24] and does not have an off–centre position as predicted by other calculations [25, 26].

For the first time, the enrichment of $P@C_{60}$ with HPLC has been investigated. The retention time between the empty and the filled molecules is t = 60 s and twice as long as for $N@C_{60}$. This is due to the higher polarisability of $P@C_{60}$. The two peaks are nearly separated and with an enrichment factor of about 30 the enrichment of $P@C_{60}$ is much faster than of $N@C_{60}$.

It was possible to measure the same sample of $P@C_{60}$ in solution and in solid state after enrichment of the material. It is the first direct demonstration of the strong broadening of the (3/2,1/2) transitions. Further experiments and a detailed discussion are presented in chapter 4.4.